Periodic structures in a one-dimensional non-linear lattice

1990 J. Phys.: Condens. Matter 2 6953

(http://iopscience.iop.org/0953-8984/2/33/008)

J. Phys.: Condens. Matter 2 (1990) 6953–6963. Printed in the UK

Periodic structures in a one-dimensional non-linear lattice

P Tchofo Dinda and E Coquet
Laboratoire OSC, Faculté des Sciences, 6 boulevard Gabriel, 21000 Dijon, France

Received 5 December 1989, in final form 2 April 1990

Abstract. We study a one-dimensional non-linear lattice with two sites per unit cell, placed respectively in a double-quadratic and a parabolic substrate potential. The phonon stability and phase diagram of this structure which can represent a possible model of some hydrogen-bonded diatomic chains are determined and some special features of the model are found.

1. Introduction and presentation of the model

Hydrogen-bonded chains have been intensively investigated with various models (Axel and Aubry 1981, Kashimori *et al* 1982, Antonchenko *et al* 1983, Zolotariuk *et al* 1984, Laedke *et al* 1985, Alexander and Krumhansl 1986, Peyrard *et al* 1987, Pnevmatikos 1988, Hochstrasser *et al* 1988). The basic hydrogen-bonded chain is a sequence of alternating heavy ions (OH^- ions in ice for instance) and protons. Two different problems are generally considered: first, the static structure of the model, i.e. its phase diagram; second, the dynamics of the protons. All the models assume a double-well substrate potential for the protons involved with the hydrogen bond but the heavy ions which are an integral part of the structure are treated differently. In the phase diagram, they are generally ignored as for instance in the approach of Axel and Aubry (1981). On the contrary the importance of the motion of the heavy ions is now well recognised (Laedke *et al* 1985, Peyrard *et al* 1987) for the dynamics of hydrogen-bonded chains since the pioneering work of Antonchenko *et al* (1983).

In this paper we investigate the role of the displacements of the heavy ions on the static structure and phase diagram. For this purpose, we consider a diatomic chain where the heavy ions move in a parabolic substrate potential representing the effect of the neighbouring lattice and where the light protons move in a double-well substrate potential with a double-quadratic form as assumed by Axel and Aubry (1981). First- and second-neighbour interactions are included in the model.

In the present work we investigate the stability and phase diagram of the model with a method similar to the method used by Coquet *et al* (1988) who investigated a two-dimensional hexagonal non-linear lattice with two sites per unit cell and an on-site double-quadratic potential. The calculations treat intrinsically the discreteness of the lattice and no continuum limit approximation is required.

0953-8984/90/336953 + 11 $03.50

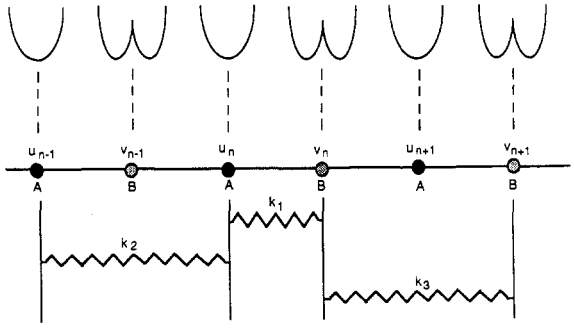

Figure 1. The non-linear lattice model defining the indices and the interaction constants.

2. Description of the model

The model is schematically shown in figure 1 where the cells are labelled by the index n. The heavy ions labelled A are submitted to the parabolic potential

$$V_{A_n} = \tfrac{1}{2}\alpha^2 u_n^2$$

where u_n denotes the displacement of the nth A atom. The light protons labelled B are submitted to the double-quadratic potential

$$V_{B_n} = \tfrac{1}{2}\mu^2[v_n - \varepsilon\sigma(n)]^2$$

where v_n denotes the displacement of the nth B atom, μ^2 measures the potential barrier, $\sigma(n) = \operatorname{sgn}(v_n)$ indicates which side of the double well is occupied and $\pm\varepsilon$ locates the two possible equilibrium positions of a B atom when the interactions between sites do not exist.

The coupling to nearest and next-nearest neighbours is described by harmonic interaction constants as indicated in figure 1. k_1 is the coupling between two adjacent A and B atoms, k_2 is the coupling between two sites of type A and k_3 is the coupling between two sites of type B. Interactions with a longer range have not been introduced in the model for simplicity.

Therefore the energy for each site in the unit cell is

$$f_{A,n} = \tfrac{1}{2}\alpha^2 u_n^2 + \tfrac{1}{4}k_1[(u_n - v_n)^2 + (u_n - v_{n-1})^2] + \tfrac{1}{4}k_2[(u_n - u_{n+1})^2 + (u_n - u_{n-1})^2] \tag{1a}$$

$$f_{B,n} = \tfrac{1}{2}\mu^2[v_n - \varepsilon\sigma(n)]^2 + \tfrac{1}{4}k_1[(u_n - v_n)^2 + (v_n - u_{n+1})^2] + \tfrac{1}{4}k_3[(v_n - v_{n+1})^2 + (v_n - v_{n-1})^2]. \tag{1b}$$

We have used here a symmetrised form of the energy per site in which half the coupling energy of an atom with its two neighbours is introduced—hence the factor $\frac{1}{4}$.

In order to reduce the number of model parameters, we have introduced reduced variables:

$$U_n = u_n/\varepsilon \qquad V_n = v_n/\varepsilon \qquad K_i = k_i/\alpha^2 \qquad (i = 1, 2, 3)$$
$$M^2 = \mu^2/\alpha^2 \qquad F_{A,n} = f_{A,n}/\alpha^2\varepsilon^2 \qquad F_{B,n} = f_{B,n}/\alpha^2\varepsilon^2.$$

In these variables, the energies per site become

$$F_{A,n} = \tfrac{1}{2}U_n^2 + \tfrac{1}{4}K_1[(U_n - V_n)^2 + (U_n - V_{n-1})^2] + \tfrac{1}{4}K_2[(U_n - U_{n+1})^2 + (U_n - U_{n-1})^2] \tag{2a}$$

$$F_{B,n} = \tfrac{1}{2}M^2[V_n - \sigma(n)]^2 + \tfrac{1}{4}K_1[(U_n - V_n)^2 + (V_n - U_{n+1})^2] + \tfrac{1}{4}K_3[(V_n - V_{n+1})^2 + (V_n - V_{n-1})^2]. \tag{2b}$$

The energy per cell is then

$$F_n = F_{A,n} + F_{B,n} \tag{3}$$

in units of $\alpha^2\varepsilon^2$, and the total energy of the chain is

$$F = \sum_n F_n. \tag{4}$$

The static structure of the model is obtained by energy minimisation, which gives the following equations for each site:

$$K_2U_{n+1} - (1 + 2K_1 + 2K_2)U_n + K_2U_{n-1} + K_1V_n + K_1V_{n-1} = 0 \tag{5a}$$

$$K_1U_{n+1} + K_1U_n + K_3V_{n+1} - (M^2 + 2K_1 + 2K_3)V_n + K_3V_{n-1} = -M^2\sigma(n). \tag{5b}$$

3. Phonon stability and the phase diagram

For a non-linear lattice, the phonon stability generally depends upon the particular phase that is considered. This is not the case for our model owing to the piecewise harmonic double-well potential. Thus we now give a general investigation of phonon stability for our model.

3.1. Phonon stability analysis

We now consider the dynamics of the model and look for solutions of the equations of motion of the chain in terms of small displacements near the equilibrium position:

$$U_n = U_n^0 + X_n(t)$$
$$V_n = V_n^0 + Y_n(t)$$

where U_n^0 and V_n^0 represent the equilibrium positions in a given phase, and $X_n(t)$ and $Y_n(t)$ are small amplitude oscillations at frequency ω:

$$X_n(t) = X\exp[\mathrm{i}(\omega t - nQ)] \tag{6a}$$

$$Y_n(t) = Y\exp[\mathrm{i}(\omega t - nQ)] \tag{6b}$$

in which Q is the component of a wavevector $\boldsymbol{Q} = Q\boldsymbol{I}^*$ in the first Brillouin zone.

The equations of motion of the two sites in cell n lead to the following equation for the frequencies:

$$\omega^4 - (C_1/m_A + C_2/m_B)\omega^2 + (1/m_A m_B)(C_1 C_2 - E^2) = 0 \tag{7}$$

in which

$$C_1 = 1 + 2K_1 + 2K_2[1 - \cos(Q)] \qquad C_2 = M^2 + 2K_1 + 2K_3[1 - \cos(Q)]$$
$$E = 2K_1 \cos(Q/2) \tag{8}$$

and m_A and m_B represent the masses of A and B atoms, respectively.

As expected, equation (7) does not depend upon $\sigma(n)$ because the phonon stability does not depend upon a particular phase as mentioned above. The lattice is linearly stable if the squares of frequencies which are roots of (7) are positive for all $\boldsymbol{Q}$ in the first Brillouin zone:

$$\omega_1^2 > 0 \qquad \omega_2^2 > 0. \tag{9}$$

We take advantage of the quadratic form of (7) to express the conditions (9) in terms of the product P of roots, the sum S of roots and the discriminant D:

$$D \geqslant 0 \qquad P = \omega_1^2 \omega_2^2 > 0 \qquad S = \omega_1^2 + \omega_2^2 > 0. \tag{10}$$

The first of these three conditions written as

$$D = (C_1 - rC_2)^2 + 4rE^2 \geqslant 0 \tag{11}$$

where $r = m_A/m_B$ is always true. In terms of the model parameters, the last two expressions give

$$\{1 + 2K_1 + 2K_2[1 - \cos(Q)]\}\{M^2 + 2K_1 + 2K_3[1 - \cos(Q)]\} - 4K_1^2 \cos^2(Q/2) > 0 \tag{12a}$$

$$1 + 2K_1 + 2K_2[1 - \cos(Q)] + r\{M^2 + 2K_1 + 2K_3[1 - \cos(Q)]\} > 0. \tag{12b}$$

We can determine analytically the limits of stability in the parameter space from conditions (12a) and (12b) at a few particular points in the Brillouin zone.

$Q = 0$ gives us the condition

$$K_1 > -M^2/2(1 + M^2). \tag{13}$$

For $Q = \pi$, two other conditions are easily obtained by (9):

$$K_1 > -\tfrac{1}{2} - 2K_2 \tag{14a}$$

$$K_1 > -M^2/2 - 2K_3. \tag{14b}$$

We note that these three conditions do not depend on r. In addition, for a given K_2, they are reduced to (13) and (14b) when $K_2 > K_{2c} = -1/4(1 + M^2)$ or (14a) and (14b) when $K_2 < K_{2c}$. Conditions (13) and (14a) are equivalent when $K_2 = K_{2c}$. We also note that a special feature of K_{2c} is that it varies from $-\frac{1}{4}$ to 0 as M^2 increases from 0 to infinity.

A numerical analysis scanning the whole Brillouin zone enables us to extend these analytical conditions and ultimately to divide the parameter space into regions of phonon stability and phonon instability. We have determined the phonon stability in the (K_1, K_3) plane for a given K_2. We have found that, when $K_2 > K_{2c}$, the phonon stability does not depend upon the particular value of K_2 that is considered and the borders of the

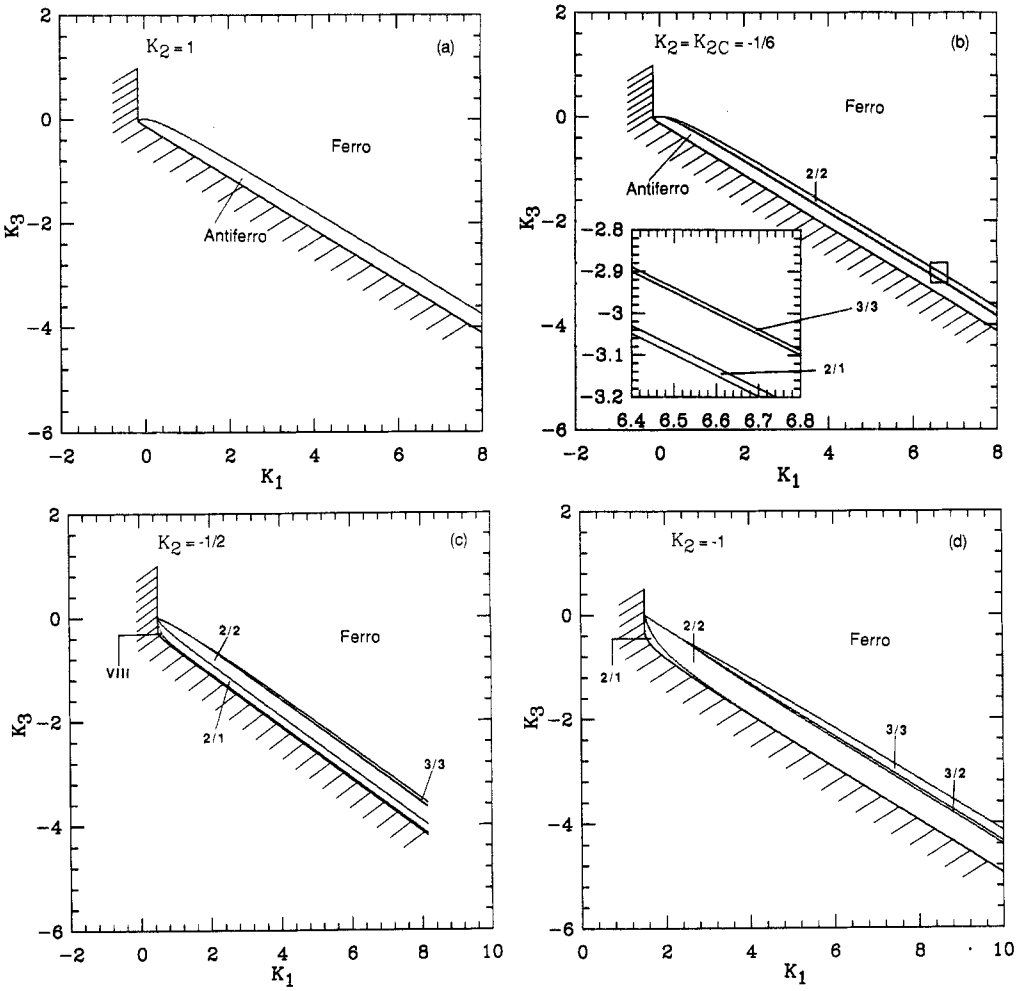

Figure 2. Plot of different plane sections (K_1, K_3) of the (K_1, K_2, K_3) phase space corresponding to K_2-values of (*a*) 1, (*b*) $-\frac{1}{6}$, (*c*) $-\frac{1}{2}$ and (*d*) -1. $M^2 = \frac{1}{2}$ throughout. The bold lines show the borders between different phases. The stability line is indicated by the shaded border. The inset in (*b*) is an enlargement of the small box shown in the figure.

stability regions are entirely determined by the two straight lines resulting from the analytical conditions (13) and (14*b*). In figure 2(*a*) the stability line is indicated by the shaded border. For $K_2 = K_{2c}$, the stability line results in a similar fashion from the two previous straight lines but the sharp intersection is replaced by a smooth curve which is only slightly visible in figure 2(*b*). When $K_2 < K_{2c}$, the phonon stability depends on K_2 and the stability line here is a straight line connected to a smooth curve as shown in figures 2(*c*) and 2(*d*). We have also found that phonon stability does not depend on the ratio r of the A and B masses.

3.2. The phase diagram

A given phase is characterised by both its period P_1 and its $\{\sigma(n)\}$ configuration. There are 2^{P_1} configurations corresponding to a given P_1 period. However, symmetry considerations reduce the number of phases to investigate. We have concentrated our

Table 1. $\{\sigma(n)\}$ configurations for phases which have been investigated.

Period	Structure	Configuration
1	I (ferro)	+
2	1/1 (antiferro)	+ −
3	2/1	+ + −
4	IV	+ + + −
	2/2	+ + − −
5	VI	+ + + + −
	3/2	+ + + − −
	VIII	+ − + − +
6	IX	+ + + + + −
	X	+ + + + − −
	XI	+ + + − + −
	3/3	+ + + − − −
	XIII	+ + − + − −

attention on the lower-period phases. However, the description of domain walls in the different phases can be used to complete the phase diagrams. We have systematically investigated all the periodic phases up to period 6. They are listed in table 1. The 1- and 1/1-phases which have the same configuration as a ferroelectric domain and an antiferroelectric domain will be called respectively ferro and antiferro states. The phases corresponding to V_n with n particles on one side of the double-well potential and n' on the other side are denoted n/n' (for instance the phase with configuration $\{+++---\}$ is denoted 4/3). This notation gives an immediate description on the configuration of a given phase.

We now present the static solutions of the atomic positions U_n and V_n for the structures which are considered. To obtain U_n and V_n, equations (5*a*) and (5*b*) are first decoupled as done by Coquet *et al* (1988). We obtain a set of higher-order finite difference equations:

$$U_{n+2} + 2AU_{n+1} + BU_n + 2AU_{n-1} + U_{n-2} = f(n) \tag{15a}$$

$$V_{n+2} + 2AV_{n+1} + BV_n + 2AV_{n-1} + V_{n-2} = g(n) \tag{15b}$$

with

$$A = \gamma_1 + \gamma_2 - \tfrac{1}{2}\beta_1\beta_2 \qquad B = 2(1 + 2\gamma_1\gamma_2 - \beta_1\beta_2) \tag{16}$$

$$f(n) = 2\delta_2\beta_1[\sigma(n) + \sigma(n-1)]$$

$$g(n) = -2\delta_2[2\gamma_1\sigma(n) + \sigma(n-1) + \sigma(n+1)] \tag{17}$$

where

$$\beta_1 = K_1/K_2 \qquad \beta_2 = K_1/K_3 \qquad \delta_1 = 1/2K_2 \qquad \delta_2 = M^2/2K_3$$
$$\gamma_1 = -1 - \delta_1 - \beta_1 \qquad \gamma_2 = -1 - \delta_2 - \beta_2. \tag{18}$$

Equation (15*b*) is formally equivalent to that of Axel and Aubry (1981). There is, however, a major difference because the right-hand side contains not only the local configuration $\sigma(n)$ at site n but also configurations at the neighbouring sites $n \pm 1$. These

extra terms reflect the coupling mediated by the heavy ions that are not present in the model used by Axel and Aubry and as discussed later it modifies the phase diagram.

Equation (15) is formally equivalent to that treated previously by Peyrard and Büttner (1987) for domain walls in a similar one-dimensional lattice model. It has also been obtained by Coquet *et al* (1988) for the quasi-one-dimensional structures of a diatomic hexagonal lattice model. For a given configuration $\{\sigma(n)\}$, this inhomogeneous difference equation can be solved exactly (Bender and Orszag 1978, Axel and Aubry 1981, Reichert and Schilling 1985, Peyrard and Büttner 1987, Coquet *et al* 1988). The general solution can be expressed in terms of the roots of the characteristic equation of the homogeneous finite-difference equation derived from (15). These roots come in pairs, the product of each pair being unity $(\nu, 1/\nu, \zeta, 1/\zeta)$, and in which ν and ζ designate the two roots with a modulus smaller than unity. The roots depend on the model parameters and can be real or complex. In terms of the roots, the solution is

$$U_n = \frac{S}{\nu - 1/\nu} \sum_{j=-\infty}^{+\infty} f(n+j)\nu^{|j|} - \frac{S}{\zeta - 1/\zeta} \sum_{j=-\infty}^{+\infty} f(n+j)\zeta^{|j|} \tag{19a}$$

$$V_n = \frac{S}{\nu - 1/\nu} \sum_{j=-\infty}^{+\infty} g(n+j)\nu^{|j|} - \frac{S}{\zeta - 1/\zeta} \sum_{j=-\infty}^{+\infty} g(n+j)\zeta^{|j|} \tag{19b}$$

with

$$S = 1/(\nu + 1/\nu - \zeta - 1/\zeta). \tag{20}$$

This configuration has, of course, to be checked for self-consistency at each site. The self-consistency condition is written as

$$\sigma_n = \mathrm{sgn}(V_n). \tag{21}$$

We shall discuss these conditions for our special solutions.

Equations (19) consist of terms containing the sums of the geometric series

$$\sum_{j=-\infty}^{+\infty} \sigma(n+j)\nu^{|j|} \qquad \text{and} \qquad \sum_{j=-\infty}^{+\infty} \sigma(n+j)\zeta^{|j|}. \tag{22}$$

For a given configuration we first calculate analytically the sums, and then we determine the atomic positions U_n and V_n. As an illustration we perform these calculations for the ferro and the antiferro states:

For the ferro state $\sigma(n) = 1$ (or -1) for all n,

$$U_n = X_1\sigma(n) \qquad V_n = Y_1\sigma(n) \tag{23}$$

where

$$X_1 = 2M^2K_1/[M^2 + 2K_1(1+M^2)] \qquad Y_1 = M^2(2K_1+1)/[M^2 + 2K_1(1+M^2)]. \tag{24}$$

We see that Y_1 is always positive when the condition (13) is fulfilled. Therefore in the whole phonon stability region the self-consistency relation (21) is satisfied by solution

(23). Using equation (3), we then calculate the average energy per cell for the ferro state:

$$E = M^2 K_1/[M^2 + 2K_1(1 + M^2)].$$

For the antiferro state $\sigma(n) = (-1)^n$,

$$U_n = 0 \qquad V_n = Y_2\sigma(n) \tag{25}$$

where

$$Y_2 = M^2/(M^2 + 2K_1 + 4K_3). \tag{26}$$

We see that Y_2 is always positive when the condition (14*b*) is fulfilled. Therefore in the whole phonon stability region the self-consistency relation (21) is satisfied by solution (25). Using equation (3), we then calculate the energy per cell for the antiferro state:

$$E = M^2(K_1 + 2K_3)/(M^2 + 2K_1 + 4K_3).$$

Although U_n, V_n and the energy of the static solutions can be evaluated analytically from equations (19) and (3) as we have done above for the ferro and antiferro states, the calculations are tedious. Therefore we have solved our equations numerically and determined the phase diagram by the following three-step process.

(i) For each set of parameters K_1, K_2, K_3, M^2 and for a given phase with period P_1, equations (15*a*), (15*b*) and (17) are rewritten with the appropriate periodicity conditions:

$$U_n = U_{n+P_1} \qquad V_n = V_{n+P_1} \qquad \sigma(n) = \sigma(n + P_1) \tag{27}$$

which give two systems of equations which can be written in terms of matrices:

$$\mathbf{T}(P_1)\boldsymbol{U} = \boldsymbol{F} \tag{28a}$$

$$\mathbf{T}(P_1)\boldsymbol{V} = \boldsymbol{G} \tag{28b}$$

where $\boldsymbol{U}$, $\boldsymbol{V}$, $\boldsymbol{F}$, $\boldsymbol{G}$ and $\mathbf{T}(P_1)$ are given in table 2. We note that $\mathbf{T}(P_1)$ is the same for all the phases with the periodicity P_1. Atomic positions U_n and V_n are finally obtained by solving (28*a*) and (28*b*). In order to avoid some difficulties in the numerical analysis the ferro and antiferro states are treated as phases with higher periods of three $\{+\,+\,+\}$ and four $\{+\,-\,+\,-\}$, respectively.

(ii) The average energy E per cell is calculated:

$$E = \left(\sum_{i=1}^{P_1} f_{A,i} + f_{B,i}\right)\Big/ P_1 \tag{29}$$

with

$$f_{A,i} = \tfrac{1}{2}U_i^2 + \tfrac{1}{4}K_1[(V_i - U_i)^2 + (U_i - V_{i-1+P_1})^2] + \tfrac{1}{4}K_2[(U_i - U_{i+1})^2 + (U_i - U_{i-1+P_1})^2] \tag{30a}$$

$$f_{B,i} = \tfrac{1}{2}M^2[V_i - \sigma(i)]^2 + \tfrac{1}{4}K_1[(V_i - U_i)^2 + (V_i - U_{i+1})^2] + \tfrac{1}{4}K_3[(V_i - V_{i+1})^2 + (V_i - V_{i-1+P_1})^2]. \tag{30b}$$

(iii) The phase which has the lowest energy and fulfils the self-consistency condition is determined.

Up to period 2, these three steps can be performed analytically and the results obtained previously for the ferro and antiferro states are preserved.

Table 2. Matrices defining the phases which have been investigated.

$$\mathbf{U} = \begin{bmatrix} U_1 \\ U_2 \\ \vdots \\ U_{P_1-1} \\ U_{P_1} \end{bmatrix} \qquad \mathbf{V} = \begin{bmatrix} V_1 \\ V_2 \\ \vdots \\ V_{P_1-1} \\ V_{P_1} \end{bmatrix} \qquad \mathbf{F} = \begin{bmatrix} f(1) \\ f(2) \\ \vdots \\ f(P_1-1) \\ f(P_1) \end{bmatrix} \qquad \mathbf{G} = \begin{bmatrix} g(1) \\ g(2) \\ \vdots \\ g(P_1-1) \\ g(P_1) \end{bmatrix}$$

$$\mathbf{T}(3) = \begin{bmatrix} B & 2A+1 & 2A+1 \\ 2A+1 & B & 2A+1 \\ 2A+1 & 2A+1 & B \end{bmatrix} \qquad \mathbf{T}(4) = \begin{bmatrix} B & 2A & 2 & 2A \\ 2A & B & 2A & 2 \\ 2 & 2A & B & 2A \\ 2A & 2 & 2A & B \end{bmatrix}$$

$$\mathbf{T}(P_1) = \begin{bmatrix} B & 2A & 1 & 0 & . & . & . & \dots & 0 & 1 & 2A \\ 2A & B & 2A & 1 & 0 & . & . & \dots & . & 0 & 1 \\ 1 & 2A & B & 2A & 1 & 0 & . & \dots & . & . & 0 \\ 0 & 1 & 2A & B & 2A & 1 & 0 & \dots & . & . & 0 \\ & & & & & & & & & & \\ \vdots & & & & & & & & & & \\ & & & & & & & & & & \\ 0 & 0 & . & & \dots & 0 & 1 & 2A & B & 2A & 1 \\ 1 & 0 & 0 & & \dots & . & 0 & 1 & 2A & B & 2A \\ 2A & 1 & 0 & & \dots & . & . & 0 & 1 & 2A & B \end{bmatrix} \quad \text{for } P_1 \geqslant 5$$

Table 3. Phases appearing in the phase diagrams with their corresponding symmetries.

Centrosymmetric configurations	Configurations with an inversion centre
+ I (ferro)	+ − 1/1 (antiferro)
+ − + 2/1	+ + − − 2/2
− + + + − 3/2	+ + + − − − 3/3
+ − + − + VIII	

In our calculations we restrict ourselves to lower M^2 values which favour the mobility of protons. First we present the results obtained for the particular value $M^2 = \frac{1}{2}$, and then we examine the effects of changing M^2.

For a given M^2, the phase space is a three-parameter space K_1, K_2, K_3. In order to display conveniently the results we shall present sections of this space corresponding to a fixed K_2, plotted in the (K_1, K_3) plane. As noticed previously for the phonon stability analysis, the value of $K_2 = K_{2c}(K_{2c} = -\frac{1}{6}$ for $M^2 = \frac{1}{2})$ plays a particular role. Therefore we discuss separately the cases $K_2 > K_{2c}$, $K_2 = K_{2c}$ and $K_2 < K_{2c}$.

As a general result we have found that only phases whose configurations have some symmetry appear in the phase diagram as ground states. Some of them are centrosymmetric; others have an inversion centre. They are shown in table 3. Fur-

thermore the self-consistency condition (21) is always satisfied in the whole parameter space where a given phase is the ground state.

When $K_2 > K_{2c}$, the phase diagrams for different K_2 do not depend upon the particular value of K_2 that is considered and therefore the different sections are identical and only the ferro and antiferro states appear (see figure 2(a)).

When K_2 becomes equal to K_{2c}, three higher-period phases lie in the transition region between the ferro and antiferro states. Those phases are the 2/1-, 2/2- and 3/3-phases. They are shown in figure 2(b). We note that the 3/3-phase appears next to the ferro state whereas the 2/1-phase appears between the 1/1- and the 2/2-phase.

For $K_2 < K_{2c}$, the phase diagrams change with K_2 unlike the case $K_2 > K_{2c}$ and the antiferro state does not appear. Figures 2(c) and 2(d) show that the 2/1-, 2/2- and 3/3-stability regions become larger. Another higher-period phase appears near the intersection of the borderlines of stability in figure 2(c). This is the VIII-phase, but it disappears when K_2 becomes sufficiently low, and only phases of type n/n and $n(n-1)$ are stable in the presence of the ferro state as shown in figure 2(d). In addition, the transition line between an n/n-phase and an $(n-1)/(n-1)$-phase splits into two lines that enclose an $n(n-1)$-phase (figure 2(d)).

From the various sections, it is easy to build up the three-dimensional phase diagram. It is interesting to note that the transition region to the ferro state occurs gradually from the antiferro state over the 2/2-phase, the 3/3-phase up to some n/n-phase with decreasing K_2. A similar result was already obtained by Büttner and Heym (1987) for the quasi-one-dimensional structures of a triangular lattice. We also notice that, as K_2 decreases, the phases near the borderlines of stability disappear gradually and the transition line between an n/n-phase and an $(n-1)/(n-1)$-phase splits into two lines that enclose an $n/(n-1)$-phase.

In order to examine the effects of the height of the double-well potential barrier, we have performed a similar study for different values of M^2. The main results of this paper for $M^2 = \frac{1}{2}$ are preserved: whenever $K_2 > K_{2c}$, only ferro and antiferro states lie in a unique phase diagram such as in figure 2(a). For $K_2 \leqslant K_{2c}$, the phase diagram depends upon the particular value of K_2 that is considered. In addition, we find that the regions corresponding to the antiferro state become larger with increasing M^2. We also notice that, as M^2 varies, K_{2c} ranges from $-\frac{1}{4}$ to 0 and so the whole positive K_2-axis corresponds to strong stability of the ferro and antiferro states.

Comparing our phase diagram with that of Axel and Aubry (1981) where the heavy ions are not taken into account, we find some interesting results; the phase diagram of our model differs qualitatively according to the value of the coupling between the heavy ions K_2. For a sufficiently strong repulsive interaction ($K_2 \leqslant K_{2c}$), the d/d′-type ground states appear in our phase diagram (see figure 2(d)). Those phases are also found by Axel and Aubry (1981) and, as in their phase diagram, with the ferro state they occupy the larger regions in our phase diagram. On the contrary, for weak repulsion or attractive interaction between the heavy ions ($K_2 > K_{2c}$), only ferro and antiferro states appear in our phase diagram which becomes therefore extremely simple (see figure 2(a)). This difference shows the crucial role of the heavy ions of the chain.

4. Conclusions

We have investigated in the present paper a possible model of hydrogen-bonded diatomic chains. The results given in figure 2 show the significant role of the K_2-coupling intro-

duced between the A atoms. For instance, as long as $K_2 > K_{2c} = -1/4(1 + M^2)$, we note an exceptional stability of the ferro and antiferro states. The independence of the phase diagram with respect to K_2 in the domain $K_2 > K_{2c}$ is a special feature of the model. On the contrary, phase diagrams plotted in the (K_1, K_3) plane for $K_2 < K_{2c}$ depend on the particular value of K_2 that is considered. As K_2 decreases, higher-period phases always appear of type n/n next to the ferro state. Their stability regions become larger and the transition line between an n/n-phase and an $(n-1)/(n-1)$-phase splits into two lines that enclose an $n/(n-1)$-phase. Some phases appear near the borderline of stability, but they ultimately disappear when K_2 becomes sufficiently low that only phases of type n/n and $n/(n-1)$ are stable in the presence of the ferro state.

We find results similar to those of Büttner and Heym (1987) about the transition regions between the ferro state and the n/n-phase. We also note that symmetries in the configurations associated with phases which are stable exist. Some of them are centrosymmetric. Others have an inversion centre.

We also find results similar to those of Axel and Aubry (1981) in the parameter regions $K_2 \leqslant K_{2c}$, unlike the case $K_2 > K_{2c}$ which favours only the ferro and antiferro states. This dependence of the phase diagram plotted in the (K_1, K_3)-plane on K_2-coupling between the heavy ions, demonstrates the role of these ions in the static structure of the model, which is also now well recognised in dynamical studies.

Nevertheless, the model that we have investigated oversimplifies the structure of the real material; a useful extension would be to substitute a more general and realistic φ^4-type potential for the double-quadratic potential. Moreover, the great displacements of the heavy ions could deform the double-well potential associated with protons as assumed in dynamical models (Zolotariuk *et al* 1984, Laedke *et al* 1985, Peyrard *et al* 1987, Hochstrasser *et al* 1988). It would also be interesting to introduce a deformable φ^4-type potential as currently done in dynamical studies of this model.

Acknowledgments

The authors would like to thank R Boesch and M Peyrard for carefully reading the manuscript.

References

Alexander D M and Krumhansl J A 1986 *Phys. Rev.* B **33** 7172
Antonchenko V Ya, Davydov A S and Zolotariuk A V 1983 *Phys. Status Solidi* b **115** 631
Axel F and Aubry S 1981 *J. Phys. C: Solid State Phys.* **14** 5433
Bender C M and Orszag S A 1978 *Advanced Mathematical Methods for Scientists and Engineers* (New York: McGraw Hill) pp 49–53
Büttner H and Heym J 1987 *Z. Phys.* B **68** 279
Coquet E, Peyrard M and Büttner H 1988 *J. Phys. C: Solid State Phys.* **21** 4895
Hochstrasser D, Büttner H, Desfontaines H and Peyrard M 1988 *Phys. Rev.* A **38** 5332
Kashimori Y, Kikuchi T and Nishimoto K 1982 *J. Chem. Phys.* **77** 1904
Laedke E W, Spatschek K H, Wilkens M Jr and Zolotariuk A V 1985 *Phys. Rev.* A **32** 1161
Peyrard M and Büttner H 1987 *J. Phys. C: Solid State Phys.* **20** 1535
Peyrard M, Pnevmatikos S and Flytzanis N 1987 *Phys. Rev.* A **36** 903
Pnevmatikos S 1988 *Phys. Rev. Lett.* **60** 1534
Reichert P and Schilling R 1985 *Phys. Rev.* B **32** 5731
Zolotariuk A V, Spatschek K H and Laedke E W 1984 *Phys. Lett.* **101A** 517